

## Supplementary Information

### Singlet oxygen from cation driven superoxide disproportionation and consequences for aprotic metal-O<sub>2</sub> batteries

Eléonore Mourad,<sup>a</sup> Yann K. Petit,<sup>a</sup> Riccardo Spezia,<sup>b</sup> Aleksej Samojlov,<sup>a</sup> Francesco F. Summa,<sup>c</sup> Christian Prehal,<sup>a</sup> Christian Leybold,<sup>a</sup> Nika Mahne,<sup>a</sup> Christian Slugovc,<sup>a</sup> Olivier Fontaine,<sup>d,e</sup> Sergio Brutti <sup>\*f</sup> and Stefan A. Freunberger <sup>\*a</sup>

<sup>a</sup>Institute for Chemistry and Technology of Materials, Graz University of Technology, Stremayrgasse 9, Graz 8010, Austria

<sup>b</sup>Laboratoire de Chimie Théorique, UMR 7616 CNRS, Sorbonne Université, CC 137, 4, Place Jussieu, 75252 Paris Cedex 05 - France

<sup>c</sup>Dipartimento di Scienze, Università della Basilicata, V.le Ateneo Lucano 10, 85100 Potenza, Italy

<sup>d</sup>Institut Charles Gerhardt Montpellier, UMR 5253, CC 1701, Université Montpellier, Place Eugène Bataillon, 34095 Montpellier Cedex 5, France

<sup>e</sup>Réseau sur le Stockage Electrochimique de l'Energie (RS2E), CNRS FR3459, 33 rue Saint Leu, 80039 Amiens, France

<sup>f</sup>Dipartimento di Chimica, Università di Roma La Sapienza. P.le A. Moro 5, 00185 Roma, Italy

#### Supplementary Methods

**Photochemical generation of <sup>1</sup>O<sub>2</sub>.** <sup>1</sup>O<sub>2</sub> was generated photochemically by illuminating O<sub>2</sub> saturated solutions containing 1 μM of the photosensitizer palladium(II) *meso*-tetra(4-fluorophenyl)tetrabenzoporphyrin (Pd<sub>4</sub>F) at a wavelength of 643 nm.<sup>1</sup> Photosensitization transfers energy from absorbed light to triplet oxygen. The process is initiated by the excitation of the photosensitizer from its S<sub>0</sub> ground state to its excited singlet state S<sub>n</sub>, which then relaxes to the lowest excited singlet state S<sub>1</sub> and yields the triplet state T<sub>1</sub> via intersystem crossing (ISC). T<sub>1</sub> then transfers the energy to <sup>3</sup>O<sub>2</sub> to form <sup>1</sup>O<sub>2</sub>.

**Measuring the quenching efficiency.** We measured the quenching efficiency by monitoring the disappearance rate of the <sup>1</sup>O<sub>2</sub> trap 9,10-dimethylantracene (DMA) in presence of the quencher during photochemical <sup>1</sup>O<sub>2</sub> generation as frequently used in the literature.<sup>2,3</sup> A hermetically sealed quartz cuvette with a 1 mL head space, equipped with a stirring bar, was filled with 1 mL of a TEGDME solution containing Pd<sub>4</sub>F and DMA in an Ar glovebox. The solution was bubbled with high purity oxygen at a flow rate of 1 mL·min<sup>-1</sup> for 20 min as well as during illumination. The cuvette was then placed in the UV-Vis spectrometer with a temperature controlled sample holder (22 °C). Prior to photooxygenation, a spectrum of the sample was recorded between 200 nm and 800 nm, to calculate the initial DMA concentration C<sub>DMA,0</sub> according to Beer-Lambert's law  $A = \varepsilon \cdot C \cdot d$  using the absorbance  $A$  at 379 nm.  $\varepsilon$  and  $d$  are extinction coefficient and light path length, respectively. Photooxygenation was performed by illuminating for a given time, followed by 60 s stirring without illumination to ensure a homogeneous solution. After each photooxidation step, an absorbance spectrum was recorded. In consideration of the photo-sensitizer self-absorbance, all recorded spectra were subject to solvent background correction and baseline correction. Photo-bleaching and reactions with singlet oxygen of the photosensitizer were not observed, as the absorbance values of the Q- and Soret-band of the photosensitizer Pd<sub>4</sub>F stayed constant over the time of the experiment. The decay of the DMA concentration was fitted to  $C =$

$C_0 \cdot \exp(-kt)$  to obtain the slope of DMA decay. The derivative  $-C_0 \cdot k$  was used to compare the efficiency of the quenchers. This allows determining the relative rate of  $^1\text{O}_2$  reacting with DMA or being quenched by dividing the DMA consumption rate with quencher by the rate without quencher.

## Supplementary Figures and Tables

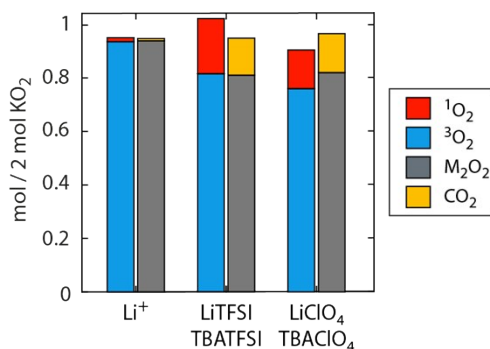


**Fig. S1** Comparison of the impact of the salt anion on disproportionation experiments. Obtained  $\text{O}_2$ ,  $^1\text{O}_2$ , and  $\text{Li}_2\text{O}_2$  upon reacting  $\text{KO}_2$  in TEGDME that contained equimolar 18-crown-6, 30 mM DMA, 0.5 M LiTFSI or  $\text{Li}^+/\text{TFSI}^+$  mixtures (5:1) with either  $\text{TFSI}^-$  for  $\text{ClO}_4^-$  as the anion. For  $\text{LiClO}_4/\text{TFSIClO}_4$  the total concentration was 0.2 M. In either case  $\text{Li}^+/\text{TBA}^+$  mixtures result in vastly increased  $^1\text{O}_2$  fractions and lower  $^3\text{O}_2$  evolution.

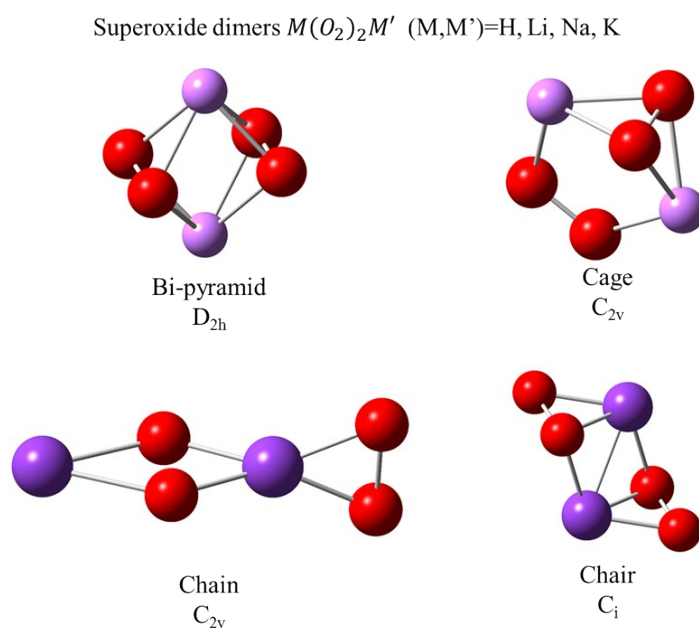


**Fig. S2** Computed structures of the neutral  $M(\text{O}_2)_2M'$  dimers with  $M, M' = \text{H}, \text{Li}, \text{Na}, \text{K}$ .

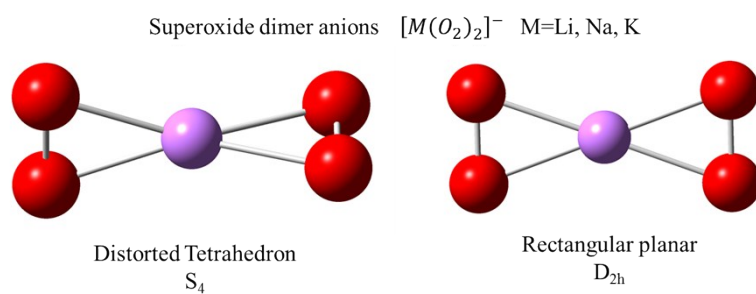


**Fig. S3** Computed structures of the  $M(O_2)_2^-$  dimer anions with  $M, M' = Li, Na, K$ .

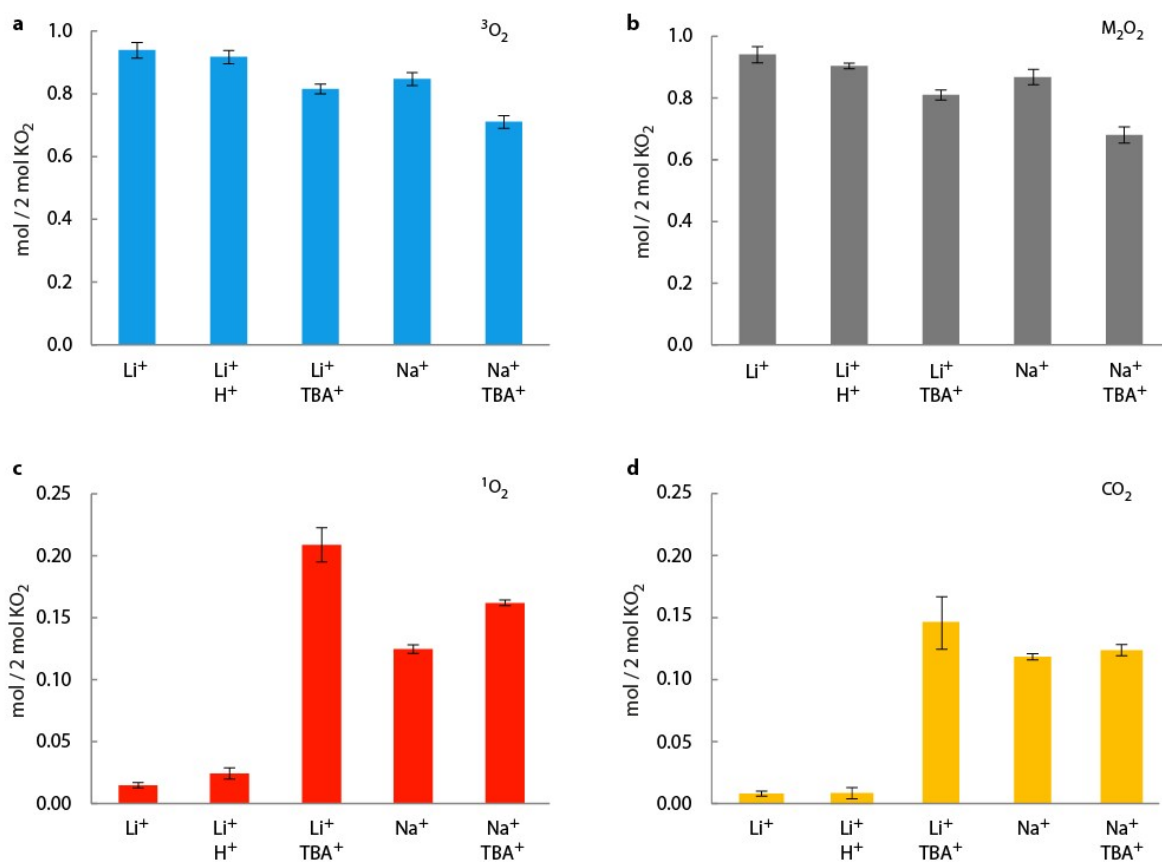


**Fig. S4** Error bars for the measurements shown in Fig. 1a. Values are obtained from at least three repetitions.

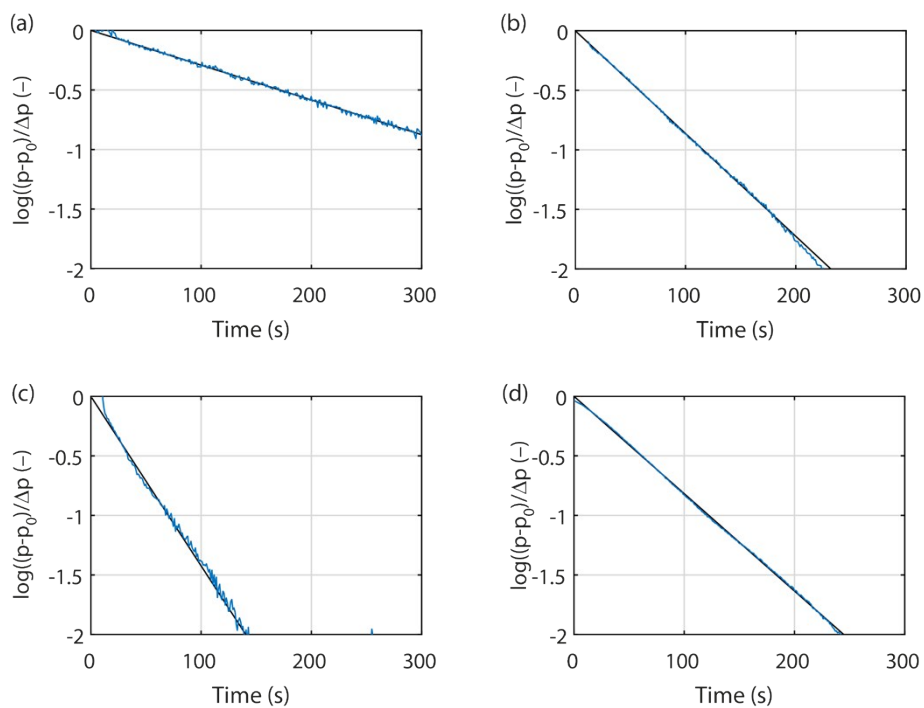


**Fig. S5** Pressure evolution during the disproportionation of  $\text{KO}_2$  solubilized by equimolar amount of 18-crown-6 in TEGDME electrolytes that contained 0.5 M  $\text{Li}^+$  and 30 mM DMA and either no additive (a) or 0.1 M  $\text{EMIm}^+$  (b),  $\text{EM}_2\text{Im}^+$  (c),  $\text{TBA}^+$  (d). Fits (black curves) are done with  $p(t) = p_0 + \Delta p(1 - e^{-kt})$ .

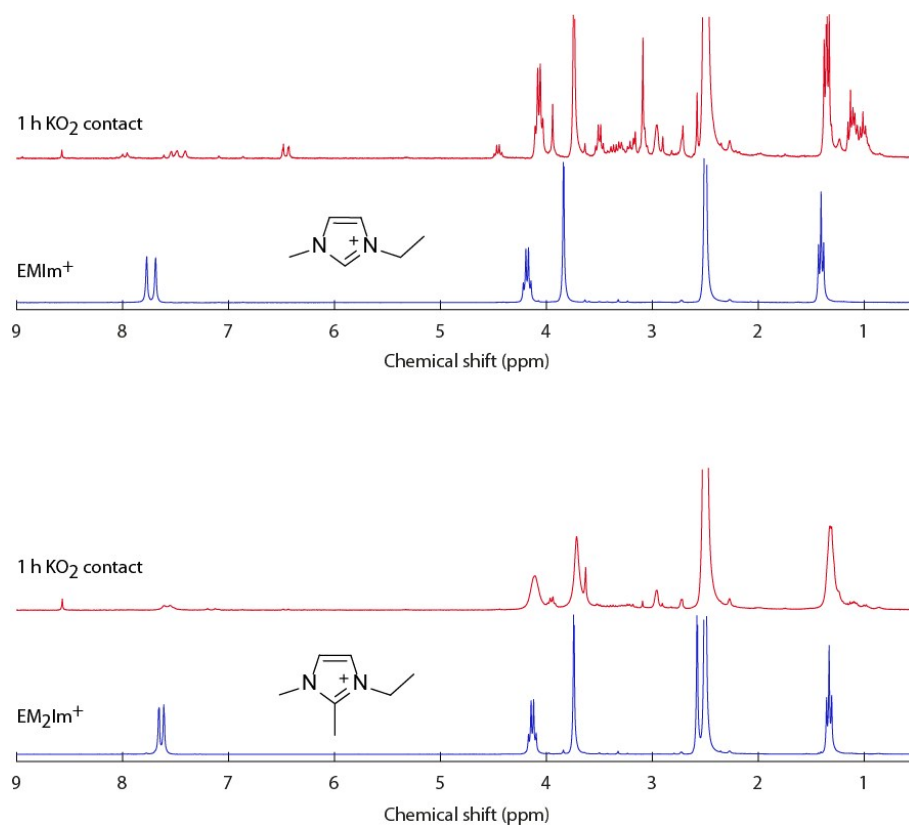


**Fig. S6**  $^1\text{H-NMR}$  spectra of  $\text{EMIm}^+$  and  $\text{EM}_2\text{Im}^+$  dissolved in TEGDME in contact with  $\text{KO}_2$  for 1 h.

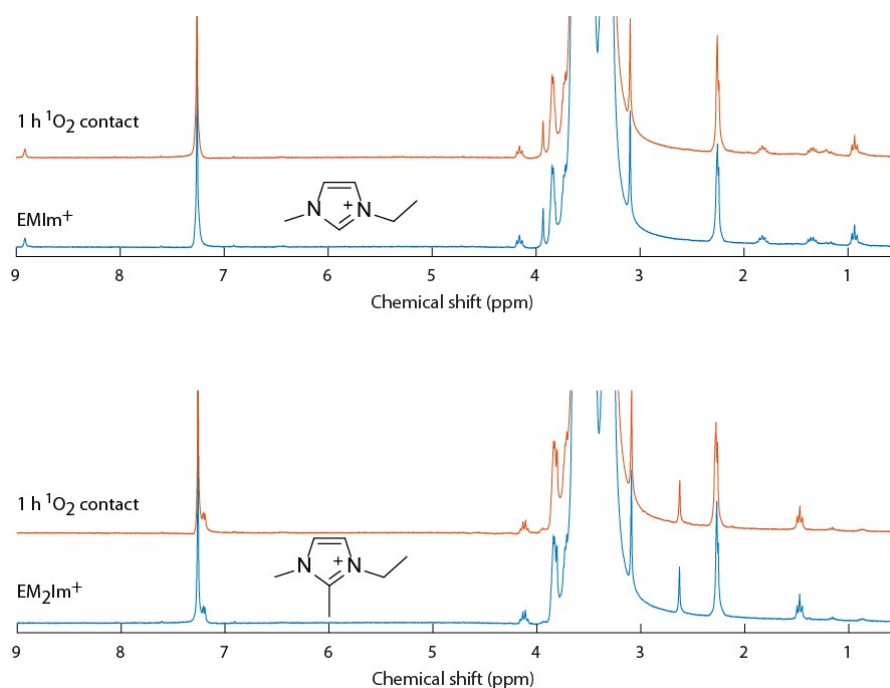


**Fig. S7**  $^1\text{H}$ -NMR spectra of  $\text{EMIm}^+$  and  $\text{EM}_2\text{Im}^+$  dissolved in TEGDME in contact with  $^1\text{O}_2$  for 1 h.  $^1\text{O}_2$  was generated photochemically by adding 1  $\mu\text{M}$  of the sensitizer palladium(II) *meso*-tetra(4-fluorophenyl)tetrabenzoporphyrin ( $\text{Pd}_4\text{F}$ ) and illuminating the  $\text{O}_2$  saturated solution at 643 nm.

### Supplementary Note 1: $^1\text{O}_2$ quenching by imidazolium

Tertiary amines are known  $^1\text{O}_2$  quenchers that physically deactivating (quench)  $^1\text{O}_2$  to  $^3\text{O}_2$ .<sup>4</sup> Imidazolium cations may hence potentially act as quenchers. If they quench they lead to an underestimation of the  $^1\text{O}_2$  amount that is derived from the DMA-to-DMA- $\text{O}_2$  conversion. We measured the quenching efficiency by monitoring the disappearance rate of the  $^1\text{O}_2$  trap DMA in absence/presence of the quenchers during continuous photochemical  $^1\text{O}_2$  generation as frequently used in the literature. Since DMA and quencher compete for reacting with/quenching  $^1\text{O}_2$ , a slower decay of DMA concentration indicates better quenching efficiency and hence a larger  $^1\text{O}_2$  fraction quenched. Fig. S4 shows that the here used imidazoliums concentration shows a noticeable quenching effect. Reported  $^1\text{O}_2$  yields with imidazoliums present are hence underestimated.

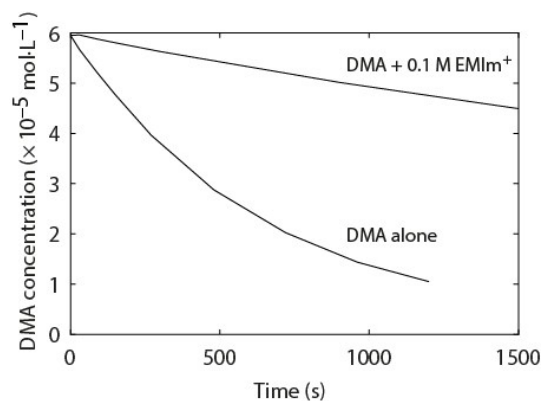


**Fig. S8** Probing the  $^1\text{O}_2$  quenching ability of  $\text{EMIm}^+$ .

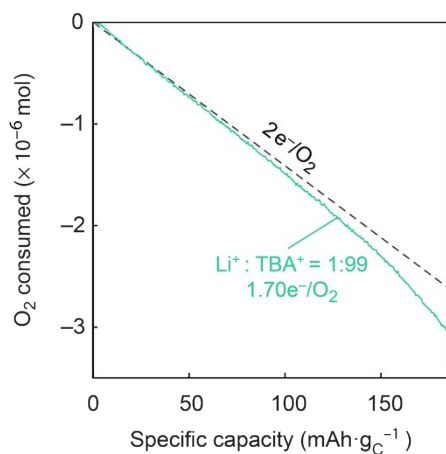


**Fig. S9** O<sub>2</sub> consumption vs. capacity upon discharge of carbon black electrodes at a rate of 100 mA·g<sup>-1</sup> in O<sub>2</sub> saturated TEGDME electrolytes that contained 30 mM DMA and a total of 1 M salt with a Li<sup>+</sup>:TBA<sup>+</sup> ratio of 1:99.

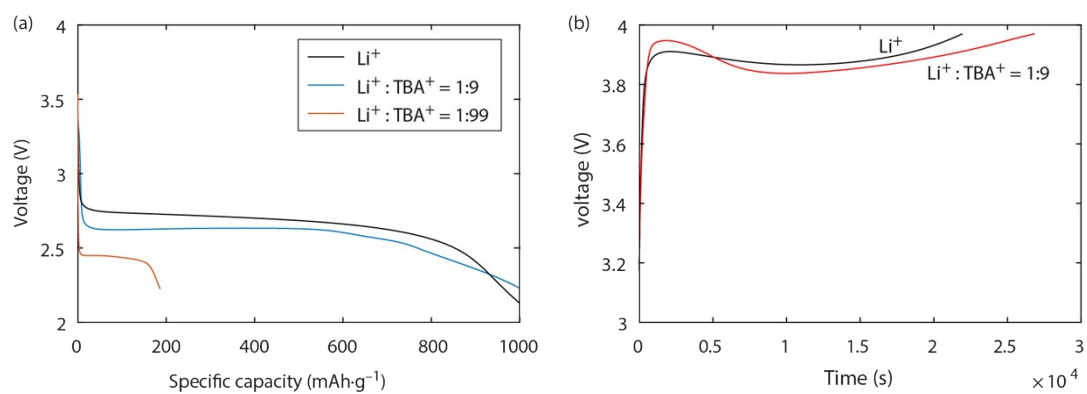


**Fig. S10** (a) Voltage versus capacity for discharge of carbon black electrodes at a rate of 100 mA·g<sup>-1</sup> in O<sub>2</sub> saturated TEGDME electrolytes that contained 30 mM DMA and either 0.1 M Li<sup>+</sup> or a total of 1 M salt with a Li<sup>+</sup>:TBA<sup>+</sup> ratio of 1:9 or 1:99. (b) Voltage vs. time upon charge of carbon black/Li<sub>2</sub>O<sub>2</sub>/PTFE (9/1/1, m/m) composite electrodes in TEGDME electrolyte containing 30 mM DMA and 0.1 M Li<sup>+</sup> (a) or 0.1 M Li<sup>+</sup> and 0.9 M TBA<sup>+</sup>. Discharge voltages drop with increasing fractions of TBA<sup>+</sup> since the electrolyte becomes increasingly viscous and O<sub>2</sub> diffusion and Li<sup>+</sup> conduction more impeded.

## Supplementary Note 2: Discharge of Li-O<sub>2</sub> cells with imidazolium cations

Figure 3 has shown that discharging a Li-O<sub>2</sub> cell with a mixed Li<sup>+</sup>/TBA<sup>+</sup> electrolyte resulted in a significantly lower e<sup>-</sup>/O<sub>2</sub> ratio of 1.74 as opposed to ~2 e<sup>-</sup>/O<sub>2</sub> for pure Li<sup>+</sup> electrolyte which came along with a drop in Li<sub>2</sub>O<sub>2</sub> yield from 94% to 85%. Using mixed Li<sup>+</sup>/EMIm<sup>+</sup> and Li<sup>+</sup>/EM<sub>2</sub>Im<sup>+</sup> electrolytes results in 1.2 and 1.42 e<sup>-</sup>/O<sub>2</sub>, respectively (Fig. S5). Concurrently, the Li<sub>2</sub>O<sub>2</sub> yields dropped to 82% with EMIm<sup>+</sup> and 85% with EM<sub>2</sub>Im<sup>+</sup> and the <sup>1</sup>O<sub>2</sub> yields increased. The even lower e<sup>-</sup>/O<sub>2</sub> compared to Li<sup>+</sup>/TBA<sup>+</sup> electrolyte is in accord with the reactivity of the imidazoliums with O<sub>2</sub><sup>-</sup> (Fig. S3), which represents an additional sink for the 1 e<sup>-</sup> product O<sub>2</sub><sup>-</sup> than a second reduction or disproportionation to <sup>3</sup>O<sub>2</sub>.

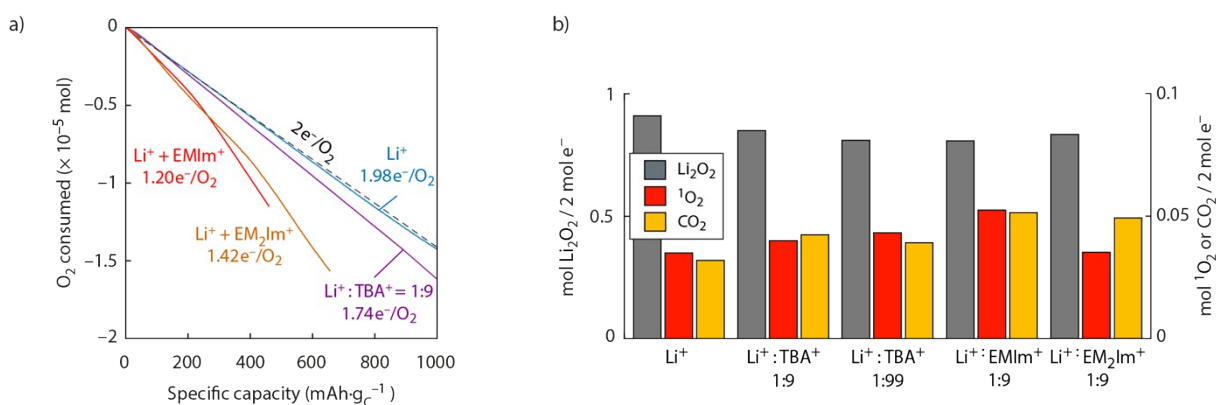


**Fig. S11** (a) O<sub>2</sub> consumption vs. capacity upon discharge of carbon black electrodes at a rate of 100 mA·g<sub>C</sub><sup>-1</sup> in O<sub>2</sub> saturated TEGDME electrolytes that contained 0.1 M Li<sup>+</sup> and 30 mM DMA and either no additive or 0.9 M TBA<sup>+</sup>, EMIm<sup>+</sup>, or EM<sub>2</sub>Im<sup>+</sup>. For TBA<sup>+</sup> also a Li<sup>+</sup>: TBA<sup>+</sup> ratio of 1:99 was measured. The 1:99 ratio is given in Fig. S9. (b) Obtained Li<sub>2</sub>O<sub>2</sub>, <sup>1</sup>O<sub>2</sub>, and Li<sub>2</sub>CO<sub>3</sub> (expressed as CO<sub>2</sub>) per 2 e<sup>-</sup> passed in the cells shown in (a).

## Supplementary Note 3: Recharge limited to 3.45 V

To exclude the suggested <sup>1</sup>O<sub>2</sub> evolution from a direct 2 e<sup>-</sup> oxidation of Li<sub>2</sub>O<sub>2</sub> above 3.5 V,<sup>5</sup> we also performed charging as in Fig. 4 with a restricted charging voltage of 3.45 V. The current was set to a relatively small value of 10 mA·g<sub>C</sub><sup>-1</sup> to reach an appreciable capacity up to 3.45 V whereafter the cell was kept at open circuit until the pressure was stable. Pressure evolution with pure Li<sup>+</sup> electrolyte (Fig. S7a) shows similarly to previous reports<sup>6-8</sup> an elevated value of 2.15 e<sup>-</sup>/O<sub>2</sub> and thus ~93% of the expected O<sub>2</sub> evolved based on charge passed. <sup>1</sup>O<sub>2</sub> formation shows that the <sup>3</sup>O<sub>2</sub> loss is connected with <sup>1</sup>O<sub>2</sub> formation. When Li<sub>2</sub>O<sub>2</sub> was charged in Li<sup>+</sup>/TBA<sup>+</sup> electrolyte (Fig. S7b), the e<sup>-</sup>/O<sub>2</sub> ratio rose to 3.77 and hence only ~53% of the expected <sup>3</sup>O<sub>2</sub> evolved. Proportional correlation between missing <sup>3</sup>O<sub>2</sub> evolution and <sup>1</sup>O<sub>2</sub> yield at either cut-off voltage suggest in either case superoxide disproportionation to be a major O<sub>2</sub> evolution and <sup>1</sup>O<sub>2</sub> generation pathway.

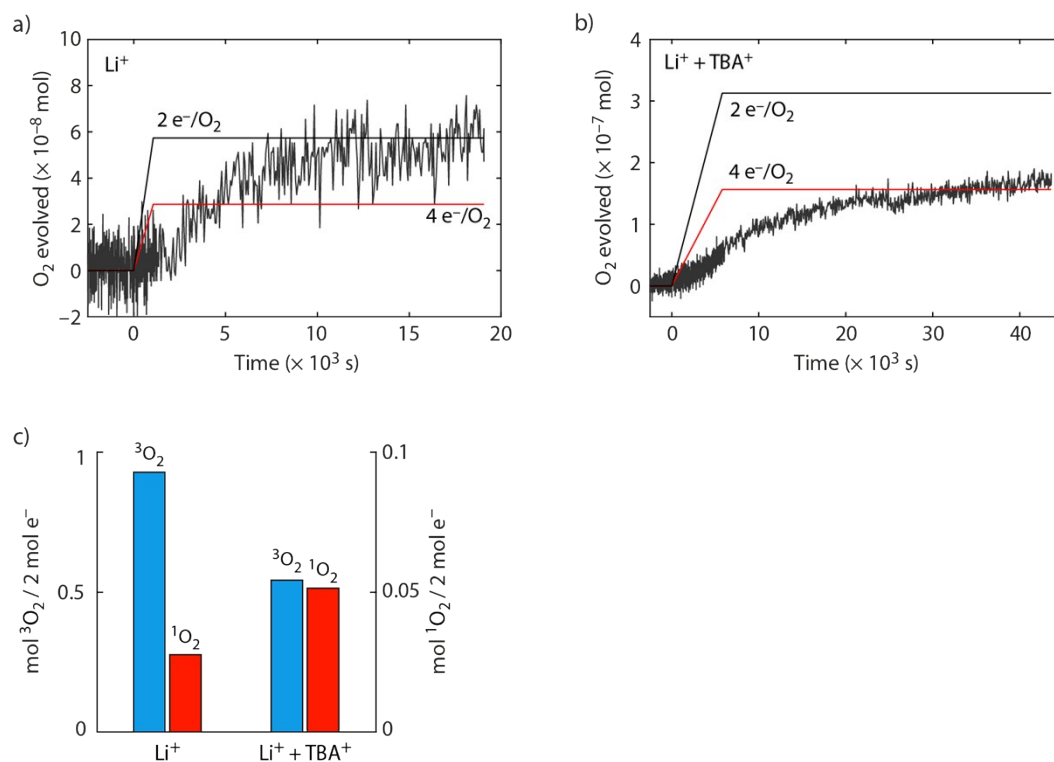


**Fig. S12** Superoxide disproportionation and <sup>1</sup>O<sub>2</sub> formation during Li-O<sub>2</sub> cell charge. (a,b) O<sub>2</sub> evolution vs. time upon charge of carbon black/Li<sub>2</sub>O<sub>2</sub>/PTFE (9/1/1, m/m) composite electrodes in TEGDME electrolyte containing 30 mM DMA and 0.1 M Li<sup>+</sup> (a) or 0.1 M Li<sup>+</sup> and 0.9 M TBA<sup>+</sup> (b). Electrodes were charged at a rate of 10 mA·g<sub>c</sub><sup>-1</sup> until 3.45 V and then kept at open circuit until the pressure was stable. (c) <sup>3</sup>O<sub>2</sub> and <sup>1</sup>O<sub>2</sub> obtained per 2 e<sup>-</sup> passed for the cells shown in (a) and (b).

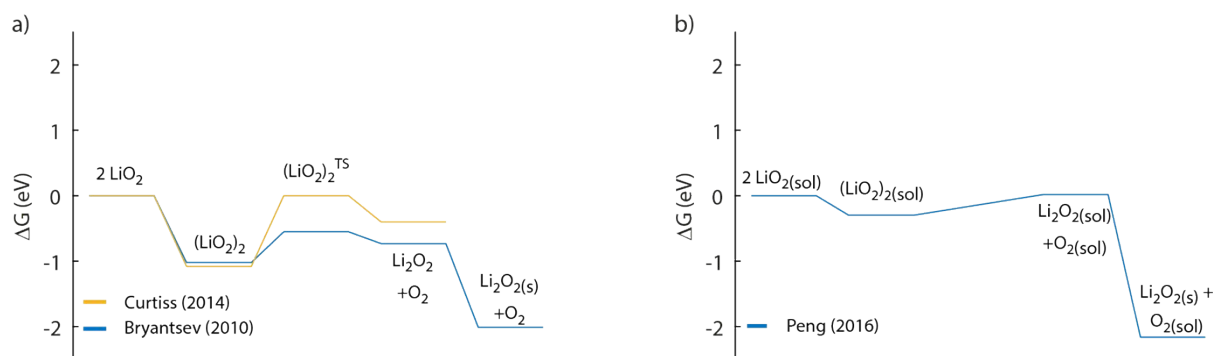


**Fig. S13** Literature reported reaction free energy profiles for <sup>3</sup>O<sub>2</sub> release from LiO<sub>2</sub> disproportionation. Species in the solvated and solid state are denoted by (sol) and (s), respectively, and in the gas phase otherwise. (a) Reactions in the gas phase as reported by Bryantsev et al.<sup>9</sup> and Curtiss et al.<sup>10</sup> Bryantsev et al. estimated the stabilization by Li<sub>2</sub>O<sub>2</sub>(s) precipitation, which is accounted for in the last step. (b) Reactions in the solution phase (DMSO) as reported by Peng et al.<sup>11</sup>

#### Supplementary Note 4: Relative stability of <sup>1</sup>M(O<sub>2</sub>)<sub>2</sub>M and <sup>3</sup>M(O<sub>2</sub>)<sub>2</sub>M dimers

The relative stability of the singlet/triplet dimers is the result of the interplay between the electrostatic interaction and direct σ/π bonding among monomers/anions/cations. In order to shed light on the trend of the singlet/triplet stabilities we carried out new calculations on the K(O<sub>2</sub>)<sub>2</sub>K adducts to complete the homologous

series with  $\text{Li}(\text{O}_2)_2\text{Li}$  and  $\text{Na}(\text{O}_2)_2\text{Na}$ . In all cases we considered and calculated four prototypical molecular geometries for both spin states (see above). Once we identified the minimum energy structures for the three symmetric dimers, we checked their vibrational stability and carried out natural bond orbital and second order perturbation theory analyses of the electron densities in order to understand the quantum-mechanical origin of the dimers/spins stability. In the following table we report the Gibbs energy differences (eV/formula unit) among the various symmetric dimers in the different structures computed in simulated solvent (C-PCM 1,1,2-trichloroethane that has a dielectric constant of 7.28 resembling glyme) at 298K, including all vibrational contributions.

**Table S1** Gibbs free energies  $\Delta G^\circ_{298\text{K}}$  (eV/formula unit) for singlet and triplet  $\text{M}(\text{O}_2)_2\text{M}$  dimers with  $\text{M} = \text{Li}, \text{Na}, \text{K}$ . Structures refer to Fig. S1.

Stoichiometry	Singlet spin state				Triplet spin state			
	Bi-pyramid	Cage	Chain	Chair	Bi-pyramid	Cage	Chain	Chair
$\text{Li}(\text{O}_2)_2\text{Li}$	1.07	*	*	*	1.23	<b>0.00</b>	*	0.01
$\text{Na}(\text{O}_2)_2\text{Na}$	<b>0.00</b>	*	*	*	0.35	*	*	*
$\text{K}(\text{O}_2)_2\text{K}$	<b>0.00</b>	*	*	0.72	0.47	*	*	*

\* vibrationally unstable (at least one imaginary vibrational frequency)

For both Na and K superoxide dimers the ground state structures are the singlet bi-pyramids whereas in the case of Li the caged triplet structure is the most stable one.

In all stable molecules with singlet spin state, the Natural Bonding Orbital (NBO) analysis suggests a  $(2p)-(2p)$  orbital overlap with bond formation between the  $(\text{O}_2)^--(\text{O}_2)^-$  fragments that in the bi-pyramidal structure are coplanar (i.e., the chair structure is a distorted bi-pyramid). On the other hand, the same bi-pyramidal structures in the triplet state are less stable for all alkaline metals superoxide dimers. NBO analysis of the bonding in the triplet bi-pyramids suggests the absence of effective orbital overlap and bond formation, whereas the second order perturbation theory (SOPT) analysis suggest that these molecules are stabilized only by electrostatic interactions. In this view, triplet bi-pyramids can be seen as electrostatic adducts whereas the singlet bi-pyramids are chemically bounded molecules.

Turning to the cage structure, this molecular structure is unstable for all the three alkaline superoxide dimers in the singlet spin state. For what concerns the triplet spin state, the only stable molecule is  ${}^3\text{Li}(\text{O}_2)_2\text{Li}$  whereas  ${}^3\text{Na}(\text{O}_2)_2\text{Na}$  and  ${}^3\text{K}(\text{O}_2)_2\text{K}$  with cage structure are thermodynamically unstable as their structural energy minima show one imaginary vibrational frequency.

NBO suggests that the  ${}^3\text{Li}(\text{O}_2)_2\text{Li}$  caged molecule is an electrostatic adduct similarly to the bi-pyramidal triplet structure due to the absence of atomic orbital overlaps to form bonds. In fact, SOPT analysis of the  ${}^3\text{Li}(\text{O}_2)_2\text{Li}$  caged molecule suggests strong lone pair donor-acceptor interactions between Li and O. Compared to the bi-pyramidal structure the Li-O distances are smaller in the caged molecule being  $\sim 1.88 \text{ \AA}$  to be compared to  $\sim 1.98 \text{ \AA}$ . Thus, the size of lithium ions allows the stabilization of the caged structure in the triplet state compared to the bi-pyramid thanks to a stronger O–Li lone pair dative interaction. We may argue that similarly due to the larger size of Na and K a similarly strong metal–O coordination does not occur and the resulting triplet caged molecules become vibrationally unstable. The intrinsic reaction coordinate analyses of the  ${}^3\text{Na}(\text{O}_2)_2\text{Na}$  and  ${}^3\text{K}(\text{O}_2)_2\text{K}$  cage energy minima suggest the adduct break-up to give the monomers.

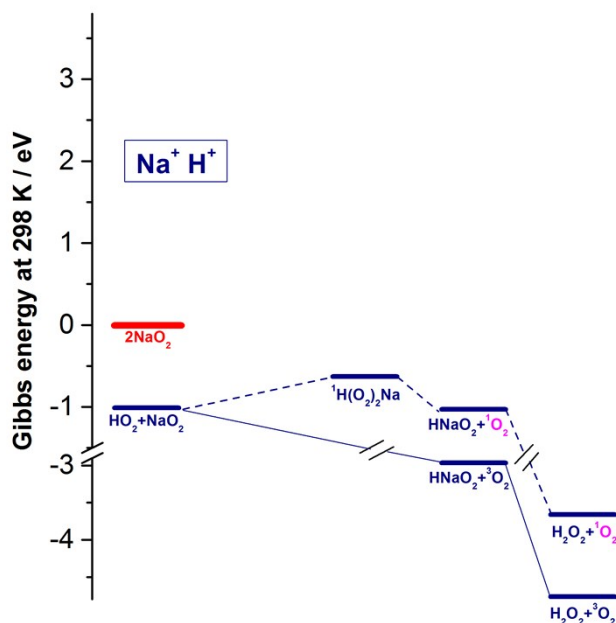


**Fig. S14** Reaction free energy profiles for asymmetric  $\text{NaO}_2\text{-HO}_2$  disproportionation. Pathways to release  $^3\text{O}_2$  and  $^1\text{O}_2$  are indicated by full and dashed lines, respectively.

**Table S2** Numerical values for the superoxide dimerization free energy  $\Delta_r G^\circ_{298\text{K}} / \text{eV}$  shown in Fig. 5. \* denotes vibrationally unstable molecules (C-PCM 1,1,2-trichloroethane that has a dielectric constant of 7.28 resembling glyme)

Stoichiometry	$\Delta_r G^\circ_{298\text{K}} (\text{eV})$	
	Singlet	Triplet
$2 \text{LiO}_2 \rightarrow \text{Li}(\text{O}_2)_2\text{Li}$	0.99	-0.08
$\text{LiO}_2 + \text{O}_2^- \rightarrow \text{Li}(\text{O}_2)_2^-$	-0.49	-0.52
$\text{LiO}_2 + \text{HO}_2 \rightarrow \text{H}(\text{O}_2)_2\text{Li}$	0.45	*
$2 \text{NaO}_2 \rightarrow \text{Na}(\text{O}_2)_2\text{Na}$	0.83	1.18
$\text{NaO}_2 + \text{O}_2^- \rightarrow \text{Na}(\text{O}_2)_2^-$	-0.29	-0.32
$\text{NaO}_2 + \text{HO}_2 \rightarrow \text{H}(\text{O}_2)_2\text{Na}$	0.38	*

**Table S3** Precipitation free energy of the solid alkaline peroxides from solvated molecules (C-PCM 1,1,2-trichloroethane that has a dielectric constant of 7.28 resembling glyme),  $\Delta_r G^\circ_{298\text{K}} / \text{kJ/mol}$ .

Peroxide	$\Delta_r G^\circ_{298\text{K}} (\text{eV})$
$\text{Li}_2\text{O}_2(\text{solvated}) \rightarrow \text{Li}_2\text{O}_2(\text{solid})$	-1.71
$\text{Na}_2\text{O}_2(\text{solvated}) \rightarrow \text{Na}_2\text{O}_2(\text{solid})$	-1.40
$\text{K}_2\text{O}_2(\text{solvated}) \rightarrow \text{K}_2\text{O}_2(\text{solid})$	-2.31

**Table S4** Free energy of the dissociation and ion exchange reactions (C-PCM 1,1,2-trichloroethane that has a dielectric constant of 7.28 resembling glyme),  $\Delta_r G_{298K}^{\circ}$  / kJ/mol.

Reaction	$\Delta_r G_{298K}^{\circ}$ / eV
$LiO_2 \rightleftharpoons Li^+ + O_2^-$	1.21
$NaO_2 \rightleftharpoons Na^+ + O_2^-$	1.36
$KO_2 \rightleftharpoons K^+ + O_2^-$	0.71
$TBAO_2 \rightleftharpoons TBA^+ + O_2^-$	0.44
$Li^+ + TFSI^- + KO_2 \rightleftharpoons LiO_2 + KTFSI$	-0.87
$Na^+ + TFSI^- + KO_2 \rightleftharpoons NaO_2 + KTFSI$	-1.02
$TBA^+ + TFSI^- + KO_2 \rightleftharpoons TBAO_2 + KTFSI$	-0.10
$Li^+ + KO_2 \rightleftharpoons LiO_2 + K^+$	-0.50
$Na^+ + KO_2 \rightleftharpoons NaO_2 + K^+$	-0.64
$TBA^+ + KO_2 \rightleftharpoons TBAO_2 + K^+$	0.27

### Supplementary Note 5: disproportionation of asymmetric alkali superoxides

Several recent works have proposed mixed alkali cation electrolytes for metal- $O_2$  cells to influence solution equilibria and hence to possibly improve cell characteristics<sup>12-16</sup>. In the following, we investigate the impact of such mixtures on the energetics of  $^1O_2$  formation. Reaction free energy profiles for the disproportionation of asymmetric pairings of  $LiO_2$  and  $NaO_2$  with the lesser Lewis acidic alkali superoxides are considered in Figures S15 to S17. These are  $LiO_2$  with  $NaO_2$  or  $KO_2$ , and  $NaO_2$  with  $KO_2$ . In general, the pathways towards both  $^3O_2$  and  $^1O_2$  are less favourable than the symmetric cases with 2  $LiO_2$  or 2  $NaO_2$ . Disproportionation to  $Li_2O_2$  or  $Na_2O_2$ , respectively, will hence more likely first involve ion exchange ( $NaO_2 + Li^+ \rightarrow LiO_2 + Na^+$  or  $KO_2 + Li^+ \rightarrow LiO_2 + K^+$ , or  $KO_2 + Na^+ \rightarrow NaO_2 + K^+$ ) and then proceed via the pathways discussed in the main text.

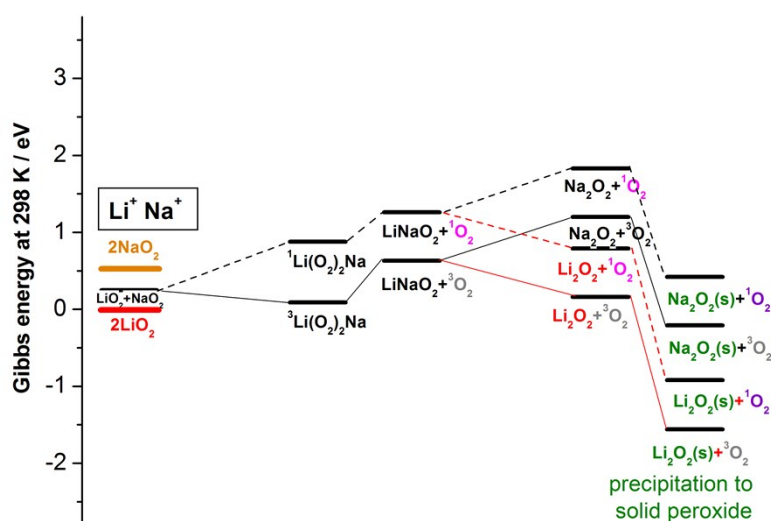


**Fig. S15** Reaction free energy profiles for asymmetric  $LiO_2 + NaO_2$  disproportionation. Pathways to release  $^3O_2$  and  $^1O_2$  are indicated by full and dashed lines, respectively.

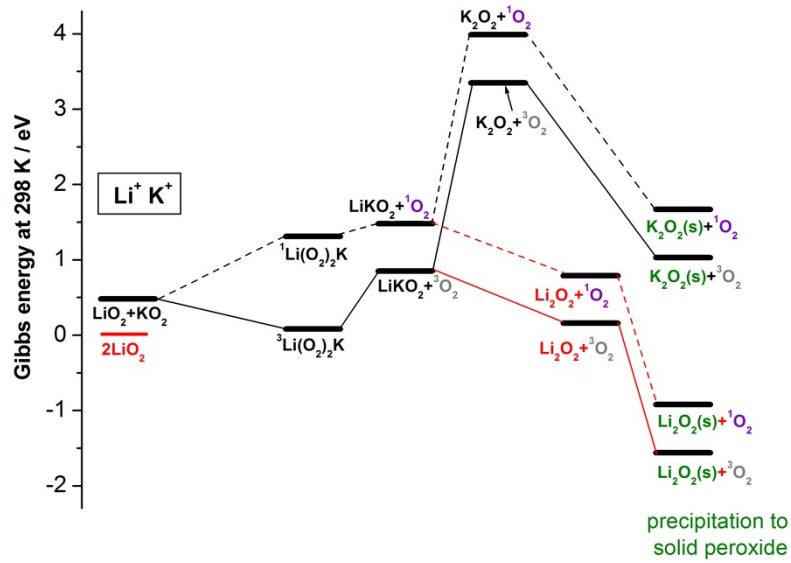


**Fig. S16** Reaction free energy profiles for asymmetric  $\text{LiO}_2 + \text{KO}_2$  disproportionation. Pathways to release  $^3\text{O}_2$  and  $^1\text{O}_2$  are indicated by full and dashed lines, respectively.

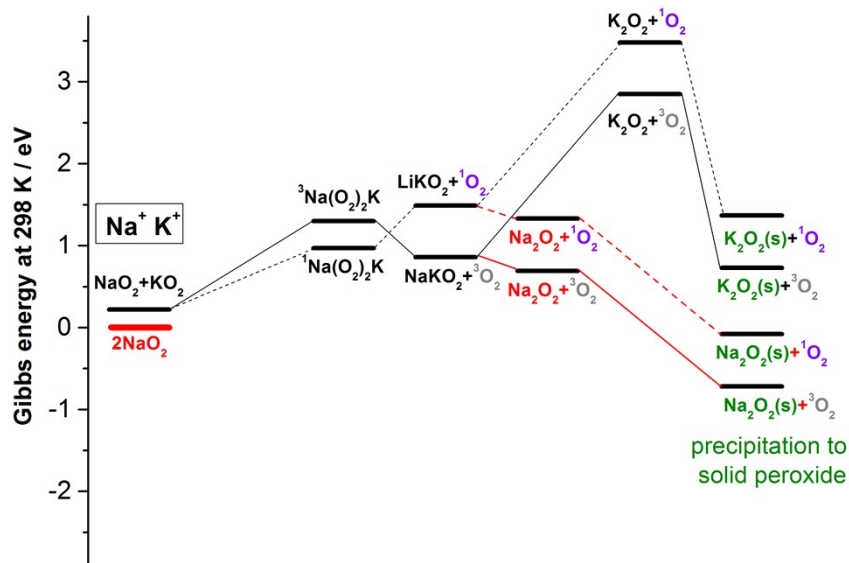


**Fig. S17** Reaction free energy profiles for asymmetric  $\text{NaO}_2 + \text{KO}_2$  disproportionation. Pathways to release  $^3\text{O}_2$  and  $^1\text{O}_2$  are indicated by full and dashed lines, respectively.

## Supplementary References

1. S. M. Borisov, G. Nuss, W. Haas, R. Saf, M. Schmuck and I. Klimant, *J. Photochem. Photobiol. A*, 2009, **201**, 128-135.
2. F. Wilkinson, W. P. Helman and A. B. Ross, *J. Phys. Chem. Ref. Data, Monograph 9, 4th ed.*, 1995, **24**, 663-1021.
3. Y. K. Petit, C. Leypold, N. Mahne, E. Mourad, L. Schafzahl, C. Slugovc, S. M. Borisov and S. A. Freunberger, *Angew. Chem. Int. Ed.*, 2019, **58**, 6535-6539.
4. C. Schweitzer and R. Schmidt, *Chem. Rev.*, 2003, **103**, 1685-1758.
5. J. Wandt, P. Jakes, J. Granwehr, H. A. Gasteiger and R.-A. Eichel, *Angew. Chem. Int. Ed.*, 2016, **55**, 6892-6895.
6. B. D. McCloskey, D. S. Bethune, R. M. Shelby, T. Mori, R. Scheffler, A. Speidel, M. Sherwood and A. C. Luntz, *J. Phys. Chem. Lett.*, 2012, **3**, 3043-3047.
7. N. B. Aetukuri, B. D. McCloskey, J. M. García, L. E. Krupp, V. Viswanathan and A. C. Luntz, *Nat. Chem.*, 2014, **7**, 50-56.
8. B. D. McCloskey, J. M. Garcia and A. C. Luntz, *J. Phys. Chem. Lett.*, 2014, **5**, 1230-1235.
9. V. S. Bryantsev, M. Blanco and F. Faglioni, *J. Phys. Chem. A*, 2010, **114**, 8165-8169.
10. U. Das, K. C. Lau, P. C. Redfern and L. A. Curtiss, *J. Phys. Chem. Lett.*, 2014, **5**, 813-819.
11. Y. Zhang, X. Zhang, J. Wang, W. C. McKee, Y. Xu and Z. Peng, *J. Phys. Chem. C*, 2016, **120**, 3690-3698.
12. J.-I. Ma, F.-I. Meng, Y. Yu, D.-p. Liu, J.-m. Yan, Y. Zhang, X.-b. Zhang and Q. Jiang, *Nat. Chem.*, 2018, **11**, 64-70.
13. I. Landa-Medrano, I. Ruiz de Larramendi and T. Rojo, *Electrochim. Acta*, 2018, **263**, 102-109.
14. I. Landa-Medrano, M. Olivares-Marín, B. Bergner, R. Pinedo, A. Sorrentino, E. Pereiro, I. Ruiz de Larramendi, J. Janek, T. Rojo and D. Tonti, *J. Phys. Chem. C*, 2017, **121**, 3822-3829.
15. C. Li, Z. Qian, Y. Ma, P. Zuo, C. Du, H. Huo and G. Yin, *New Journal of Chemistry*, 2018, **42**, 17311-17316.
16. W. Yu, H. Wang, L. Qin, J. Hu, L. Liu, B. Li, D. Zhai and F. Kang, *ACS Appl. Mater. Interf.*, 2018, **10**, 17156-17166.